Chapter 2
Discretized Feedback Systems

2.1 Introduction

As we described in the previous chapter, since discretized/quantized feedback systems become nonlinear, the analysis and design of those types of systems has not been elucidated. The first attempt to clarify these problems was described in a paper of Kalman [3]. However, few results have been obtained for the stability analysis of nonlinear discrete-time feedback systems [2, 9]. In this chapter, the analysis in an ℓ_2 space for such a discrete-time and discrete-value system is discussed.

2.2 Discretized Control Systems

A discretized nonlinear control system can be represented by a sampled-data control system with two samplers, S_1, S_2, and a continuous nonlinear characteristic, $N(\cdot)$, as shown in Fig. 2.1. Here, $\mathcal{D}_1$, $\mathcal{D}_2$, and $\mathcal{H}$ denote the discretization and zero-order hold elements, which are usually performed in A/D (D/A) conversion, and $G(s)$ is the transfer function (the Laplace-transformed one) of a linear (continuous-time) controlled system. It is assumed that the two samplers with sampling period h operate synchronously. The feedback structure corresponds to the sampling/holding system shown in Fig. 1.16, when $G_1(s)$ is considered to be a static nonlinear characteristic. The sampled-data control system can be equivalently transformed into a discretized control system, as shown in Fig. 2.2. Here, $G(z)$ is the z-transform of $G(s)$ together with a zero-order hold, and $\mathcal{D}_1$ and $\mathcal{D}_2$ are the discretizing units (static quantizers) on the input and output sides of the nonlinear element, respectively.

In Fig. 2.2, each symbol $e, u, v, \ldots$ indicates the sequence $e(k), u(k), v(k), \ldots, (k = 0, 1, 2, \cdots)$ in discrete time, but in continuous values. On the other hand, each symbol $e^\dagger, u^\dagger, v^\dagger, \ldots$ indicates a discrete value that can be assigned to an integer number, e.g.,

$$e^\dagger \in \{\cdots, -3\gamma_1, -2\gamma_1, -\gamma_1, 0,\ \gamma_1,\ 2\gamma_1,\ 3\gamma_1, \cdots\},$$

Y. Okuyama, *Discrete Control Systems*,
DOI 10.1007/978-1-4471-5667-3_2, © Springer-Verlag London 2014

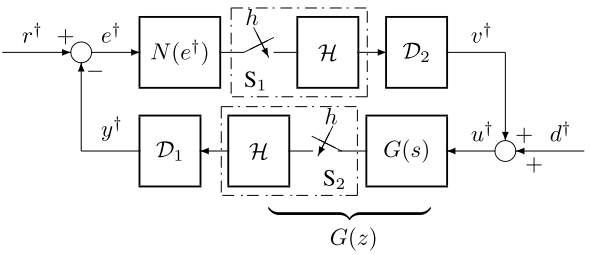

Fig. 2.1 Nonlinear sampled-data feedback system

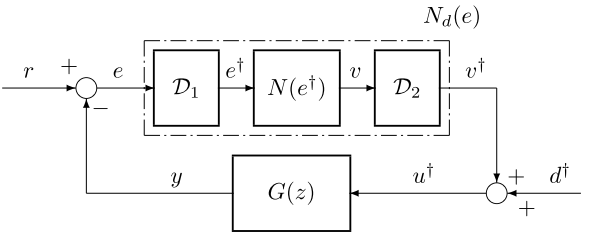

Fig. 2.2 Discretized nonlinear control system

$$v^\dagger \in \{\cdots, -3\gamma_2, -2\gamma_2, -\gamma_2, 0,\ \gamma_2,\ 2\gamma_2,\ 3\gamma_2, \cdots\},$$

where γ_1 and γ_2 are the resolution values of each variable. In the above expressions, it is assumed that the input and output signals of the nonlinearity have the same resolution in the discretization (i.e., $\gamma = \gamma_1 = \gamma_2 > 0$) [1, 5, 6]. Here, $e^\dagger$, $u^\dagger$, and $v^\dagger$ also represent the time sequences $e^\dagger(k)$, $u^\dagger(k)$, and $v^\dagger(k)$.

The relationship between e and $v^\dagger = N_d(e)$ in the figure becomes a stepwise nonlinear characteristic on integer grid coordinates, as shown in Fig. 2.3(a). In this chapter, a round-down discretization, which is usually executed on a computer, is

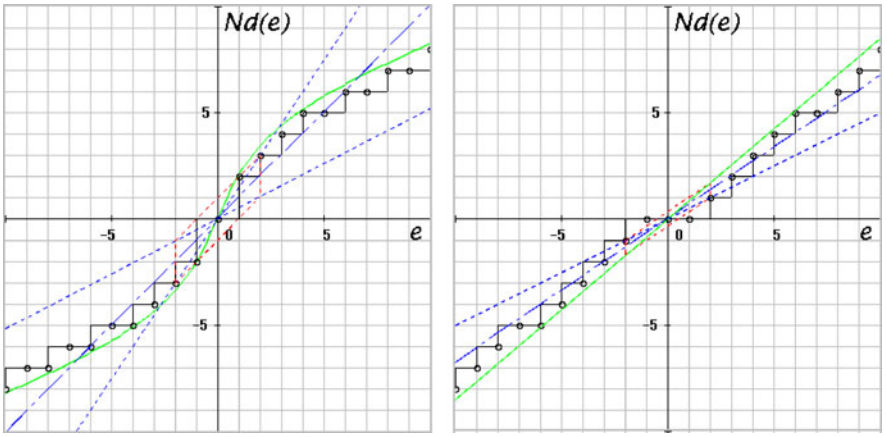

(a) (b)

Fig. 2.3 Discretization for nonlinear and linear characteristics

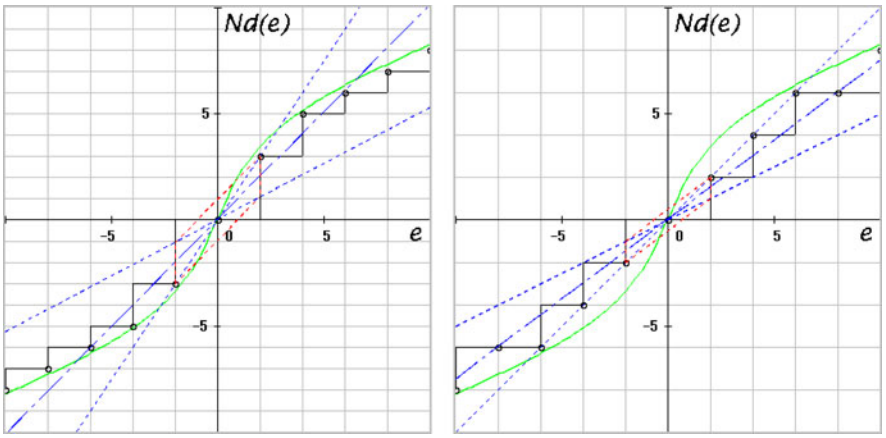

(a) (b)

Fig. 2.4 Effect of resolution values

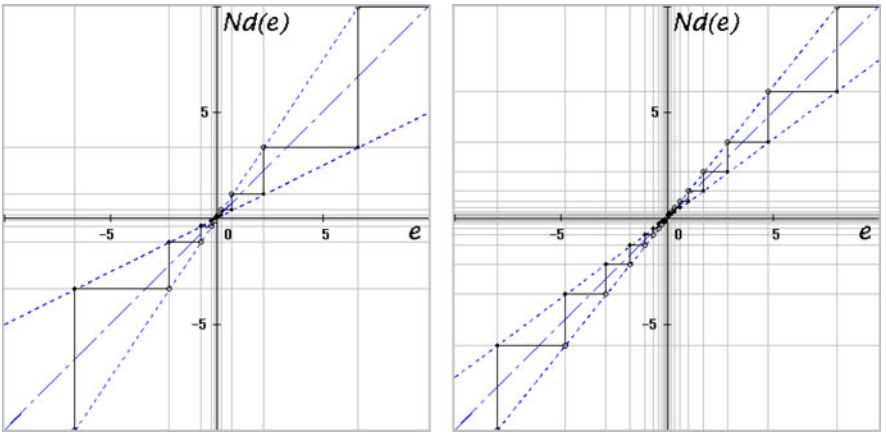

(a) (b)

Fig. 2.5 Logarithmic quantizers

applied. Therefore, the relationship between e and $v^{\dagger}$ is indicated by small circles (i.e., a point-to-point transition) on the stepwise nonlinear characteristic. Even if the continuous characteristic $N(\cdot)$ is linear, the discretized characteristic $v^{\dagger}$ becomes nonlinear on integer grid coordinates, as shown in Fig. 2.3(b). In order to compare the discretization, Figs. 2.4(a) and (b) show the effect of resolution values. In these figures, two cases are depicted: (a) input resolution $\gamma = 2$ and output resolution $\gamma = 1$, (b) input and output resolutions $\gamma = 2$.

Some authors have investigated a logarithmic quantizer in relation to the robust stability. Figs. 2.5(a) and (b) show two cases of the logarithmic quantizer. However, the applications of these discretizations are scarcely known in practice.

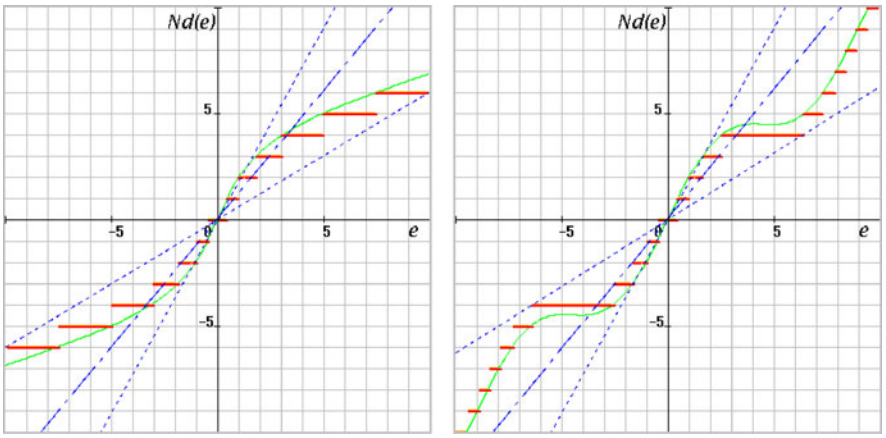

(a) (b)

Fig. 2.6 Nonlinear characteristics and output-side discretizations

Hereafter, without loss of generality, it will be assumed that $\gamma = 1$. That is, the variables $e^\dagger, u^\dagger, \cdots$ are defined by integers as follows:

$$e^\dagger, u^\dagger \in \mathbb{Z}, \qquad \mathbb{Z} := \{\cdots -3, -2, -1, 0, 1, 2, 3, \cdots\}. \tag{2.1}$$

On the other hand, the time variable t is given as $t \in \{0, h, 2h, 3h, \cdots\}$ for the sampling period h. When assuming $h = 1.0$, the following expression can be defined:

$$t \in \mathbb{Z}_+, \qquad \mathbb{Z}_+ := \{0, 1, 2, 3, \cdots\}. \tag{2.2}$$

Therefore, each signal $e^\dagger(t), u^\dagger(t), \cdots$ traces on a grid pattern that is composed of integers in the time and (controller variables) space.

2.3 Discretization and Nonlinear Sector

2.3.1 Three Types of Discretization

Output-Side Discretization When a signal is discretized only on the output side of the nonlinear characteristic, the relationship between e and $v^\dagger$ becomes a stepwise nonlinear characteristic with step height 1, as shown in Figs. 2.6(a) and (b). Figure 2.6(a) is the output-side discretization for a saturation-type nonlinear characteristic (arctangent sigmoid function). On the other hand, Fig. 2.6(b) is the output-side discretization for a sinusoidal nonlinear characteristic. Without loss of generality, it is assumed that the nonlinear characteristics have origin symmetry and exist in the first and third quadrants.

Input-Side Discretization When a signal is discretized only on the input side of the nonlinear characteristic, the relationship between e and $v^\dagger$ becomes a stepwise

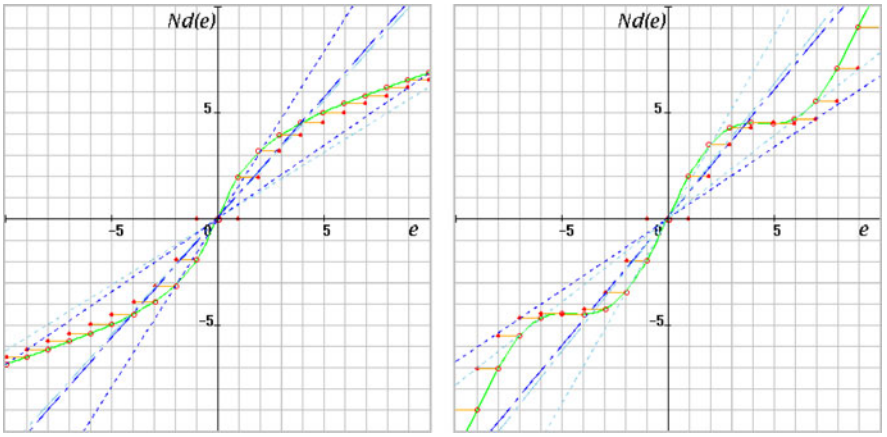

(a) (b)

Fig. 2.7 Nonlinear characteristics and input-side discretizations

nonlinear characteristic with step width 1, as shown in Figs. 2.7(a) and (b). Figure 2.7(a) is the input-side discretization for a saturation-type nonlinear characteristic (arctangent sigmoid function), whereas Fig. 2.7(b) is the input-side discretization for a sinusoidal nonlinear characteristic.

Input and Output Sides Discretization When a signal is discretized on the input and output sides of the nonlinear characteristic, the relationship between e and $v^\dagger$ becomes a stepwise nonlinear characteristic with step hight and width 1 (i.e., broken line on integer coordinates) as shown in Figs. 2.8(a) and (b). Figure 2.8(a) is the input and output side discretization for a saturation-type nonlinear characteristic (arctangent sigmoid function). On the other hand, Fig. 2.8(b) is the input and output side discretization for a sinusoidal nonlinear characteristic.

2.3.2 Nominal Gains and Sector Parameters

In general, the discretized nonlinear characteristic

$$v^\dagger = N_d(e) = Ke + g(e), \qquad 0 < K < \infty, \tag{2.3}$$

can be partitioned into the following two sections:

$$|g(e)| \le \overline{g} < \infty, \tag{2.4}$$

for $|e| < \varepsilon$, and

$$|g(e)| \le \beta |e|, \qquad 0 \le \beta \le K, \tag{2.5}$$

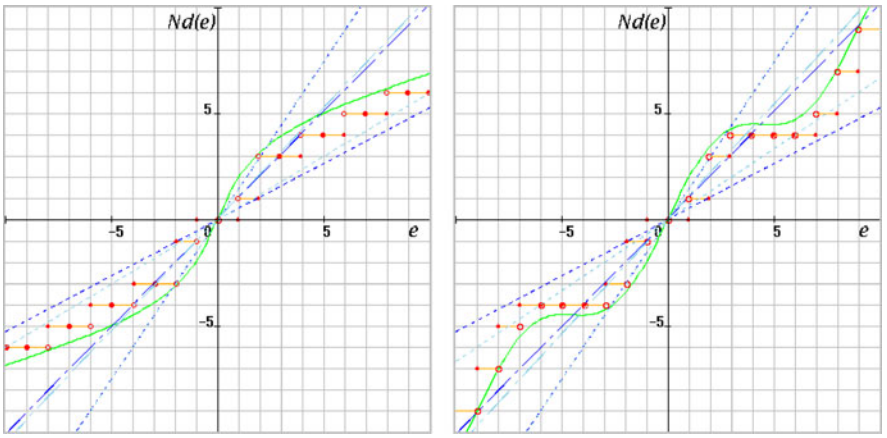

(a) (b)

Fig. 2.8 Nonlinear characteristics and input and output side discretizations

for $|e| \geq \varepsilon$. When considering relative nonlinear characteristics, the partitioned expression is given as follows:

$$v^{\dagger} = N_d(e) = K(e + n(e)),$$
$$|n(e)| \leq \alpha |e|. \tag{2.6}$$

Clearly, the sector parameter is considered to be $\beta = K\alpha$.

Equation (2.4) represents a bounded nonlinear characteristic that exists in a finite region. On the other hand, Eq. (2.5) represents a sectorial nonlinearity for which the equivalent linear gain exists in a limited range. It can also be expressed as follows:

$$0 \leq g(e)e \leq \beta e^2. \tag{2.7}$$

When dealing with the robust stability in a global sense, it is sufficient to consider the nonlinear term (2.5) for $|e| \geq \varepsilon$ because the nonlinear term (2.4) can be treated as a disturbance signal. (In the stability problem, a fluctuation or an offset of error is assumed to be allowable in $|e| < \varepsilon$.) Figures 2.9(a) and (b) show the discretization characteristics and the nonlinear parts $g(e)$ of two examples. In these examples, the thresholds are chosen as $\varepsilon = 2$.

In partitioning (2.3), nominal gain K and sectorial nonlinearity $g(e)$ can be chosen appropriately. For example, if K is chosen in integer numbers, $w^{\dagger} = g(e)$ also becomes an integer number. Figures 2.10(a) and (b) show examples of the partitioning of nonlinear characteristics when $K = 1$ (i.e., an integer number). In these cases, sector parameter β should be given by the larger value of $K_{\max} - K$ and $K - K_{\min}$. In general, the nominal gain and the sector parameter should be determined as follows:

$$K = \frac{K_{\max} + K_{\min}}{2} \tag{2.8}$$

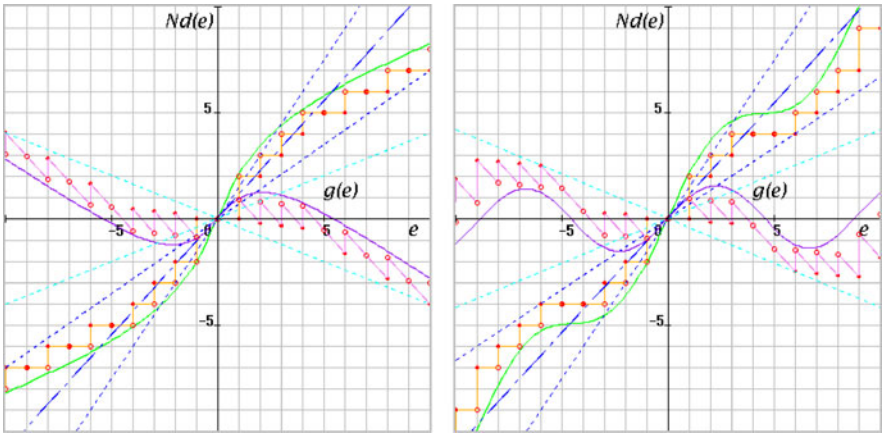

Fig. 2.9 Nonlinear characteristics and discretized outputs

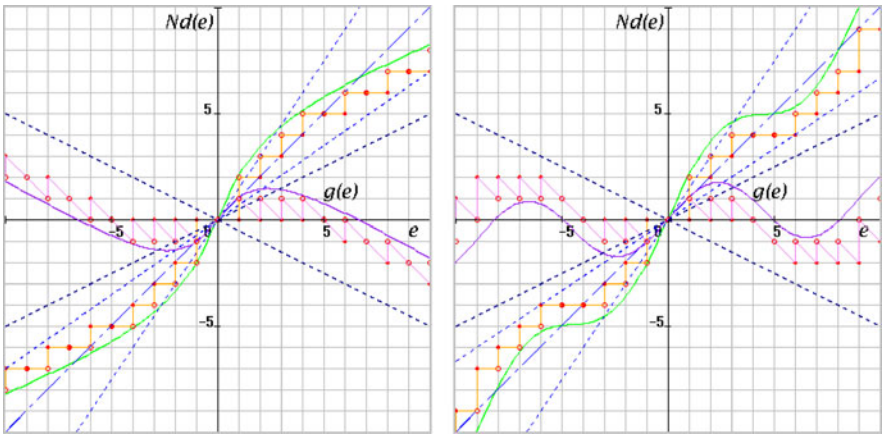

Fig. 2.10 Nonlinear characteristics and discretized outputs

$$\beta = \frac{K_{\max} - K_{\min}}{2} = K_{\max} - K. \tag{2.9}$$

By partitioning nonlinear characteristic $N_d(\cdot)$, a single-loop control system can be drawn as shown in Fig. 2.11. It can also be drawn in regard to the discretized input as shown in Fig. 2.12. In the figure, discretized input $e^\dagger$ is assumed to be determined as follows:

$$e = e^\dagger, \quad \text{when} \quad e^\dagger \le e < e^\dagger + \gamma.$$

In this case, the nominal gain and the sector parameter will be given as follows:

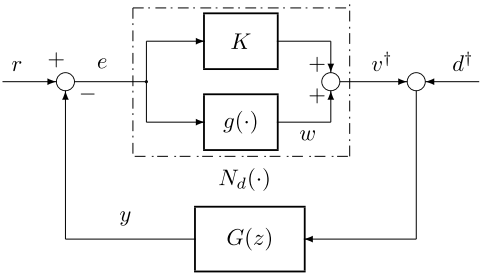

Fig. 2.11 Discretized nonlinear control system

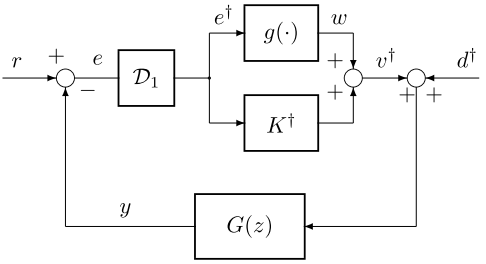

Fig. 2.12 Discrete-input nonlinear control system

$$K_n^\dagger = \frac{K_{\max}^\dagger + K_{\min}^\dagger}{2}, \tag{2.10}$$

$$\beta^\dagger = \frac{K_{\max}^\dagger - K_{\min}^\dagger}{2}, \tag{2.11}$$

where the following relations hold:[1]

$$K_{\max}^\dagger = K_{\max}, \quad K_{\min}^\dagger \le K_{\min}.$$

Figure 2.13(a) shows the difference between $K_{\min}$ and $K_{\min}^\dagger$ for the sinusoidal nonlinearity shown in Figs. 2.9(b) and 2.10(b). In this figure, nominal gains K and $K^\dagger$ are also drawn in chain lines. The control system shown in Fig. 2.12 can also be drawn as shown in Fig. 2.14. From Fig. 2.14, the relationship between $e(k)$ and $e^\dagger(k)$ and the equivalent exogenous input $\epsilon(k)$ are drawn in Fig. 2.13(b). As is clear from the figure, $\epsilon(k) = e^\dagger(k) - e(k)$ may be considered a bounded disturbance signal.

[1] β will be used instead of $\beta^\dagger$ in the following discussion.

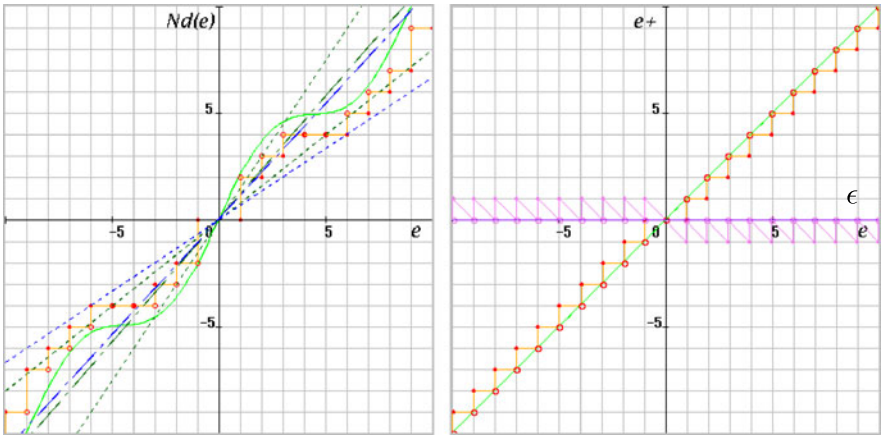

Fig. 2.13 Different sectors and equivalent input

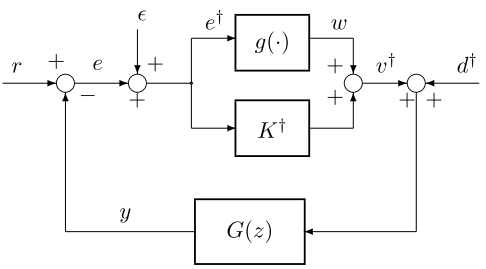

Fig. 2.14 Equivalent discrete-input control system

2.4 Equivalent Transformation

Based on the above considerations, the following new sequences $\overline{e}^*(k)$ and $\overline{w}^*(k)$ are defined:

$$\overline{e}^*(k) = \overline{e}(k) + q \cdot \frac{\Delta e(k)}{h}, \tag{2.12}$$

$$\overline{w}^*(k) = \overline{w}(k) - \beta q \cdot \frac{\Delta e(k)}{h}, \tag{2.13}$$

where q is a non-negative number, $\overline{e}(k)$ and $\overline{w}(k)$ are neutral points of sequences $e(k)$ and $w(k)$,

$$\overline{e}(k) = \frac{e(k) + e(k-1)}{2}, \tag{2.14}$$

$$\overline{w}(k) = \frac{w(k) + w(k-1)}{2}, \tag{2.15}$$

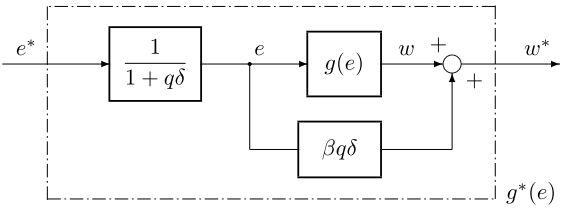

Fig. 2.15 Transformation of nonlinear element $g(e)$

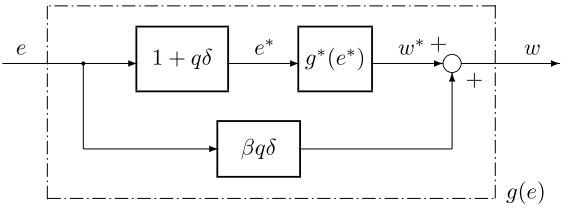

Fig. 2.16 Equivalent nonlinear subsystem

and $\Delta e(k)$ is the backward difference of sequence $e(k)$, that is,

$$\Delta e(k) := e(k) - e(k-1). \tag{2.16}$$

When using delay operator z^{-1}, Eqs. (2.14), (2.15), and (2.16) may be given as follows:

$$\overline{e}(k) = \frac{(1+z^{-1})}{2} e(k), \tag{2.17}$$

$$\overline{w}(k) = \frac{(1+z^{-1})}{2} w(k), \tag{2.18}$$

and then

$$\Delta e(k) = (1-z^{-1})\, e(k). \tag{2.19}$$

By using z-transform expressions, Eqs. (2.12) and (2.13) can be written as follows:

$$\frac{(1+z^{-1})}{2}\hat{e}^*(z) = \frac{(1+z^{-1})}{2}\hat{e}(z) + q \cdot \frac{(1-z^{-1})}{h}\hat{e}(z), \tag{2.20}$$

$$\frac{(1+z^{-1})}{2}\hat{w}^*(z) = \frac{(1+z^{-1})}{2}\hat{w}(z) - \beta q \cdot \frac{(1-z^{-1})}{h}\hat{e}(z). \tag{2.21}$$

The relationship between Eqs. (2.20) and (2.21) is shown by the block diagram in Fig. 2.15, and by the equivalent subsystem in Fig. 2.16. In these figures, operator δ is defined by a bilinear transformation as follows:

$$\delta(z) := \frac{2}{h} \cdot \frac{1-z^{-1}}{1+z^{-1}}. \tag{2.22}$$

Therefore, if the subsystem shown in Fig. 2.16 is used instead of $g(e)$, the whole control system is drawn as shown in Fig. 2.17. The control system represented by

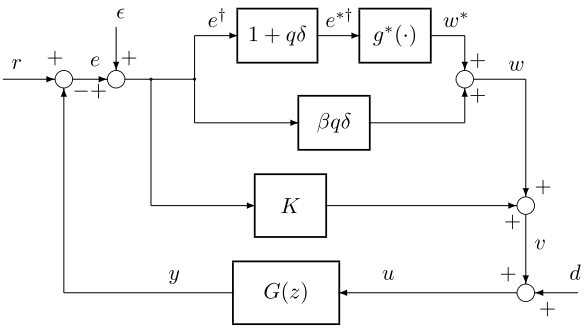

Fig. 2.17 Discrete nonlinear control system

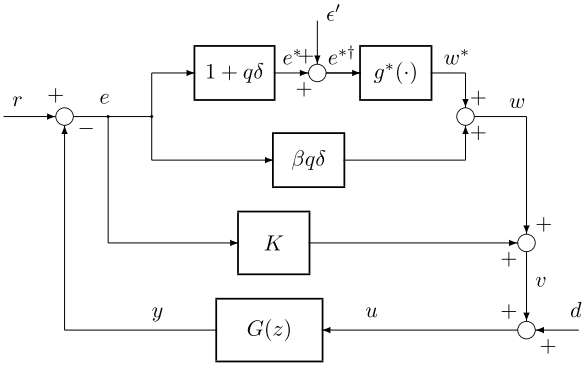

Fig. 2.18 Discrete nonlinear control system 2

Fig. 2.17 is equivalently transformed into Fig. 2.18. In this figure, since

$$\begin{cases} \hat{e}^\dagger(z) = \hat{e}(z) + \hat{\epsilon}(z) \\ \hat{e}^{*\dagger}(z) = (1 + q\delta(z))\hat{e}^\dagger(z), \end{cases}$$

the equivalent exogenous input ϵ' can be given by

$$\hat{\epsilon}'(z) = (1 + q\delta(z))\hat{\epsilon}(z). \tag{2.23}$$

From these figures,

$$\hat{e}(z) = \hat{r}(z) - G(z)[\hat{w}^*(z) + (K + \beta q\delta(z))\hat{e}(z) + \hat{d}'(z)].$$

Furthermore,

$$[1 + (K + \beta q\delta(z)]G(z)\hat{e}(z) = G(z)\hat{w}^*(z) + \hat{r}(z) + G(z)\hat{d}'(z).$$

Thus,

$$\hat{e}(z) = \frac{G(z)\hat{w}^*(z) + \hat{r}(z) + G(z)\hat{d}'(z)}{1 + (K + \beta q\delta(z))G(z)}.$$

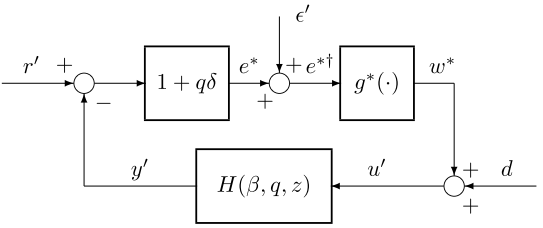

Fig. 2.19 Equivalent nonlinear control system

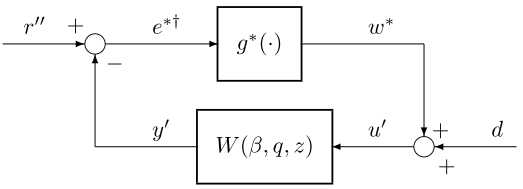

Fig. 2.20 Small-gain feedback system

From these equations, we can obtain

$$\hat{e}^*(z) = \frac{(1+q\delta(z))G(z)}{1+(K+\beta q\delta(z))G(z)}\hat{w}^*(z)$$
$$+\frac{(1+q\delta(z))}{1+(K+\beta q\delta(z))G(z)}\hat{r}(z) + \frac{(1+q\delta(z))G(z)}{1+(K+\beta q\delta(z))G(z)}\hat{d}(z). \tag{2.24}$$

Therefore,

$$e^{*\dagger}(z) = \frac{(1+q\delta(z))G(z)}{1+(K+\beta q\delta(z))G(z)}\hat{w}^*(z) + \hat{\epsilon}'(z)$$
$$+\frac{1+q\delta(z)}{1+(K+\beta q\delta(z))G(z)}\hat{r}(z) + \frac{(1+q\delta(z))G(z)}{1+(K+\beta q\delta(z))G(z)}\hat{d}(z) \tag{2.25}$$

Consequently, we have the block diagram of the discretized control system shown in Fig. 2.19, where

$$H(\beta,q,z) = \frac{G(z)}{1+(K+\beta q\delta(z))G(z)}. \tag{2.26}$$

Thus, the loop transfer function from w^* to e^* can be given by

$$W(\beta,q,z) = \frac{(1+q\delta(z))G(z)}{1+(K+\beta q\delta(z))G(z)}, \tag{2.27}$$

as shown in Fig. 2.20. Here, r' is given by

$$\hat{r}'(z) = \frac{1}{1+(K+\beta q\delta(z))G(z)}\hat{r}(z).$$

Furthermore, the reference input r'' in Fig. 2.20 is equivalently expressed as

$$\hat{r}''(z) = (1 + q\delta(z))\hat{r}'(z) + \hat{\epsilon}(z).$$

2.5 Norm Inequalities

We now provide an assumption with respect to the behavior of control systems.

Assumption The absolute value of the backward difference of sequence $e(k)$ does not exceed γ, i.e.,

$$|\Delta e(k)| = |e(k) - e(k-1)| \leq \gamma. \tag{2.28}$$

If condition (2.28) is satisfied, $\Delta e(k)$ becomes exactly $\pm\gamma$ or 0 because of the discretization $\mathcal{D}_1$. That is, the absolute value of the backward difference can be given as

$$|\Delta e(k)| = |e(k) - e(k-1)| = \gamma \ \text{ or } \ 0.$$

The assumption stated above will be satisfied in some examples given in the following chapters. These examples will include figures illustrating the phase trace of the backward difference Δe.

In this subsection, some lemmas with respect to an ℓ_2 norm of the sequences are presented. Here, we define a new nonlinear function

$$f(e) := g(e) + \beta\, e. \tag{2.29}$$

When considering the discretized output of the nonlinear characteristic, $w^\dagger = v^\dagger - Ke^\dagger$, the following expression can be given:

$$f(e^\dagger(k)) = w^\dagger(k) + \beta e^\dagger(k). \tag{2.30}$$

In expression (2.30), we note that $w^\dagger \notin \mathbb{Z}$ in general. From inequality (2.5), it can be seen that the function (2.30) belongs to the first and third quadrants. Figures 2.21(a) and (b) show the discretized outputs $v^\dagger = N_d(e)$ and $f(e)$ for the examples given in Fig. 2.9(a) and (b) when the discretized error ϵ was not considered and the point-to-point transition was executed.

Considering the equivalent linear characteristic, the following inequality can be defined:

$$0 \leq \psi(k) := \frac{f(e(k))}{e(k)} \leq 2\beta. \tag{2.31}$$

When this type of nonlinearity $\psi(k)$ is used, inequality (2.5) can be written as

$$w^\dagger(k) = g(e(k)) = (\psi(k) - \beta)e(k). \tag{2.32}$$

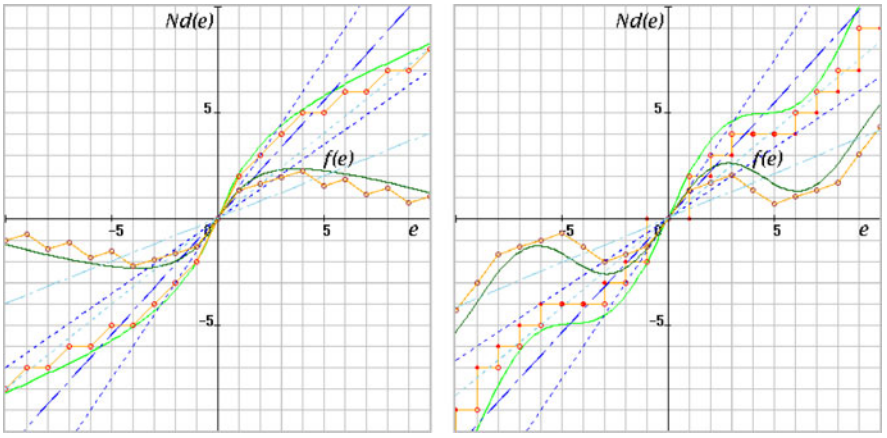

(a) (b)

Fig. 2.21 Nonlinear characteristics and discretized outputs

For the neutral points of $e(k)$ and $w^{\dagger}(k)$, the following expression is given from (2.30):

$$\frac{1}{2}(f(e(k)) + f(e(k-1))) = \overline{w}^{\dagger}(k) + \beta\overline{e}^{\dagger}(k). \tag{2.33}$$

Moreover, Eq. (2.32) is rewritten as $\overline{w}^{\dagger}(k) = (\psi(k) - \beta)\overline{e}^{\dagger}(k)$. Since $|\overline{e}^{\dagger}(k)| \leq |\overline{e}(k)|$, the following inequality is satisfied when a round-down discretization is executed:

$$|\overline{w}^{\dagger}(k)| \leq \beta|\overline{e}^{\dagger}(k)| \leq \beta|\overline{e}(k)|. \tag{2.34}$$

Based on this premise, the following norm conditions are examined.

Lemma 2.1 *The following inequality holds for a positive integer p*:

$$\|\overline{w}^{\dagger}(k)\|_{2,N} \leq \beta\|\overline{e}^{\dagger}(k)\|_{2,N} \leq \beta\|\overline{e}(k)\|_{2,N}. \tag{2.35}$$

Here, $\|\cdot\|_{2,N}$ denotes an ℓ_2 norm, which can be defined by

$$\|x(k)\|_{2,N} := \left(\sum_{k=1}^{N} |x(k)|^2\right)^{1/2}.$$

Proof The proof is clear from inequality (2.34). □

Lemma 2.2 *If the following inequality is satisfied with respect to the inner product of the neutral points of* (2.30) *and the backward difference*:

$$\left\langle \overline{w}^{\dagger}(k) + \beta\overline{e}^{\dagger}(k), \Delta e(k) \right\rangle_N \geq 0, \tag{2.36}$$

we can obtain the inequality

$$\|\overline{w}^{*\dagger}(k)\|_{2,N} \leq \beta \|\overline{e}^{*\dagger}(k)\|_{2,N} \tag{2.37}$$

for any $q \geq 0$. *Here,* $\langle \cdot, \cdot \rangle_N$ *denotes the inner product, which is defined as*

$$\left\langle x_1(k), x_2(k) \right\rangle_N = \sum_{k=1}^{N} x_1(k) x_2(k).$$

Proof The following equation is obtained from (2.12) and (2.13):

$$\begin{aligned} &\beta^2 \|\overline{e}^{*\dagger}(k)\|_{2,N}^2 - \|\overline{w}^{*\dagger}(k)\|_{2,N}^2 \\ &= \beta^2 \|\overline{e}^{\dagger}(k)\|_{2,N}^2 - \|\overline{w}^{\dagger}(k)\|_{2,N}^2 + \frac{2\beta q}{h} \cdot \left\langle \overline{w}^{\dagger}(k) + \beta \overline{e}^{\dagger}(k), \Delta e(k) \right\rangle_N. \end{aligned} \tag{2.38}$$

Thus, inequality (2.37) is satisfied by using the left-side inequality of (2.35). Moreover, as for the input of $g^*(\cdot)$, the following inequality can be obtained from (2.38) and the right-side inequality of (2.35):

$$\|\overline{w}^{*\dagger}(k)\|_{2,N} \leq \beta \|\overline{e}^{*}(k)\|_{2,N}. \tag{2.39}$$

□

2.6 Sum of Trapezoidal Areas

The left side of inequality (2.36) can be expressed by a sum of trapezoidal areas.

Lemma 2.3 *For any step* N, *the following equation is satisfied*:

$$\sigma(N) := \left\langle \overline{w}^{\dagger}(k) + \beta \overline{e}^{\dagger}(k), \Delta e(k) \right\rangle_N = \frac{1}{2} \sum_{k=1}^{N} (f(e(k)) + f(e(k-1))) \Delta e(k). \tag{2.40}$$

Proof The proof is clear from (2.33). □

In general, the sum of trapezoidal areas has the following property.

Lemma 2.4 *If inequality* (2.28) *is satisfied with respect to the discretization of the control system, the sum of trapezoidal areas becomes non-negative for any* N, *that is*,

$$\sigma(N) \geq 0. \tag{2.41}$$

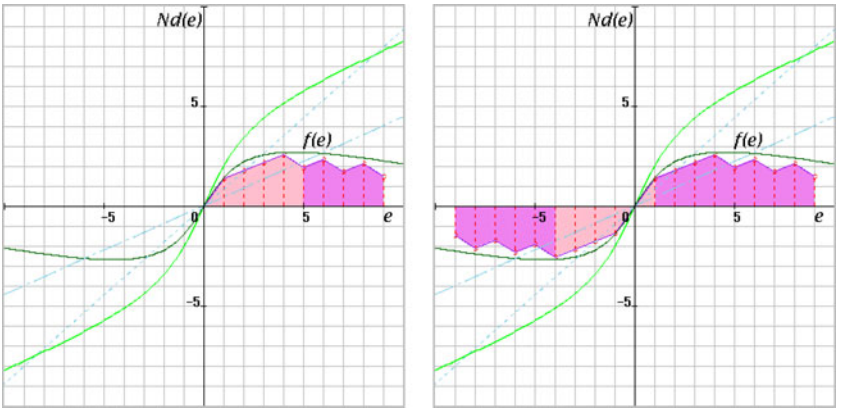

(a) (b)

Fig. 2.22 Non-negative characteristics of trapezoidal summation

Proof Since $f(e(k))$ belongs to the first and third quadrants, the area of each trapezoid

$$\tau(k) := \frac{1}{2}(f(e(k)) + f(e(k-1)))\Delta e(k) \tag{2.42}$$

is non-negative when $e(k)$ increases (decreases) in the first (third) quadrant. On the other hand, the trapezoidal area $\tau(k)$ is non-positive when $e(k)$ decreases (increases) in the first (third) quadrant.

Strictly speaking, when ($e(k) \geq 0$ and $\Delta e(k) \geq 0$) or ($e(k) \leq 0$ and $\Delta e(k) \leq 0$), $\tau(k)$ is non-negative for any k. On the other hand, when ($e(k) \geq 0$ and $\Delta e(k) \leq 0$) or ($e(k) \leq 0$ and $\Delta e(k) \geq 0$), $\tau(k)$ is non-positive for any k. Here, $\Delta e(k) \geq 0$ corresponds to $\Delta e(k) = \gamma$ or 0 (and $\Delta e(k) \leq 0$ corresponds to $\Delta e(k) = -\gamma$ or 0) for the discretized signal, when inequality (2.28) is satisfied. The sum of trapezoidal areas is given from (2.40) as:

$$\sigma(N) = \sum_{k=1}^{N} \tau(k). \tag{2.43}$$

We thus derive the following result. The sum of trapezoidal areas becomes non-negative, $\sigma(N) \geq 0$, regardless of whether $e(k)$ (and $e(k)$) increases or decreases. Since the discretized output traces the same points on the stepwise nonlinear characteristic, the sum of trapezoidal areas is canceled when $e(k)$ (and $e(k)$ decreases (increases) from a certain point $(e(k), f(e(k)))$ in the first (third) quadrant. (Here, without loss of generality, the response of discretized point $(e(k), f(e(k)))$ is assumed to commence at the origin.) Thus, the proof is concluded. □

Figures 2.22(a) and (b) show the sum of trapezoidal areas for $f(e)$ given in Fig. 2.21(a), when e is a sinusoidal input with amplitude 8.0, i.e., $e(k) = 8.0 \sin \omega k$ (ω: an arbitrary number).

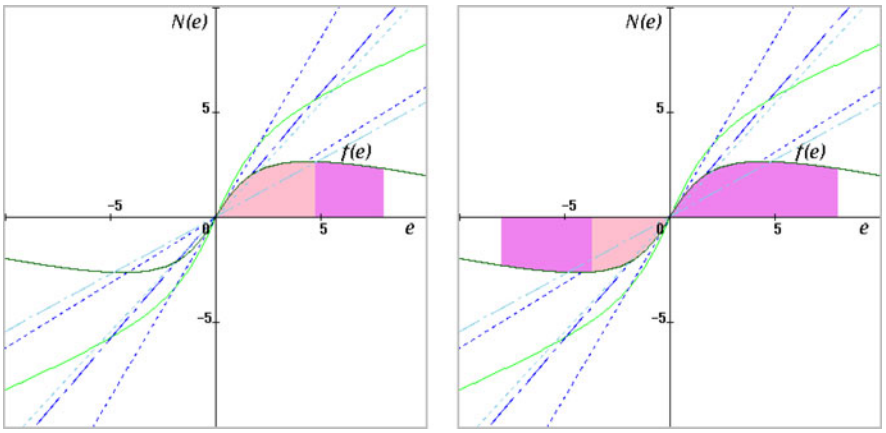

(a) (b)

Fig. 2.23 Non-negative characteristics of integrals

(a) The sinusoid starts from 0 to 8.0. Then, e decreases to $e < 5.0$.
(b) The sinusoid starts from 0, passes 8.0, 0.0, -8.0, and increases to $e > -5.0$.

In any case, the sum of trapezoids will be canceled.

On the other hand, Figs. 2.23(a) and (b) show the sum of trapezoidal areas for $f(e)$ when the sampling period h is very small (i.e., $\Delta e(k) \to 0$), in other words, the integration of $f(e)$,

$$\sigma(N) = \int_{e(0)}^{e(N)} f(e)de.$$

The latter case corresponds to the Popov stability problem for continuous control systems.[2]

For an easier understanding, examples of the sequences of continuous/discretized signals and the sum of trapezoidal areas are depicted in Figs. 2.24(a), (b) and 2.25(a), (b).

Example 2.1 The input/output characteristic shown in Fig. 2.24(a) is written as:

$$\begin{aligned} e^{\dagger} &= \gamma * (\texttt{double})(\texttt{int})(e/\gamma) \\ v &= 0.3 * e^{\dagger} + 2.7 * \texttt{atan}(0.7 * e^{\dagger}) \\ v^{\dagger} &= \gamma * (\texttt{double})(\texttt{int})(v/\gamma) \end{aligned} \tag{2.44}$$

by using a C-language expression. Here, (int) and (double) denote the conversion into an integral number (a round-down discretization) and the reconversion into a

[2]The relation to the Popov criterion will be described in Chap. 3, Sect. 3.6.

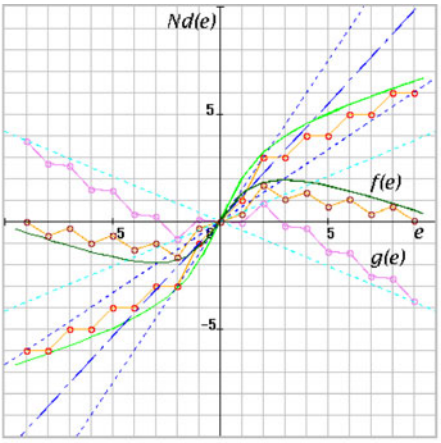

(a)

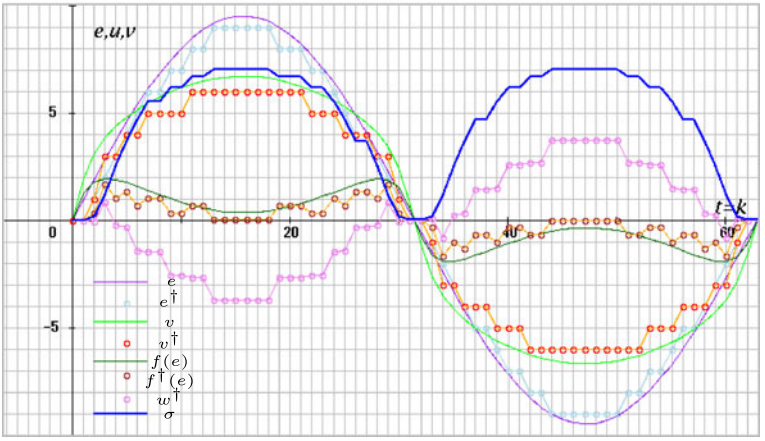

(b)

Fig. 2.24 Discretized input/output signals of a nonlinear element

double-precision real number, respectively. The second equation of (2.44) corresponds to a sigmoid (saturated) function (needless to say, $\texttt{atan}(\cdot) = \tan^{-1}(\cdot)$).

In Fig. 2.24(b), the curve e and the sequence of circles $e^\dagger$ show the input of the nonlinear element and its discretized signal. The curve v and the sequence of circles $v^\dagger$ show the corresponding output of the nonlinear characteristic and its discretized signal, respectively. As shown in the figure, the sequences of circles $e^\dagger$ and $v^\dagger$ trace a grid pattern that is composed of integers. The sequence of circles $w^\dagger$ shows the discretized output of the nonlinear characteristic $g(\cdot)$. The curve of shifted nonlinear characteristic $f(e)$ and the sequence of circles $f^\dagger(e)$ are also shown in the figures.

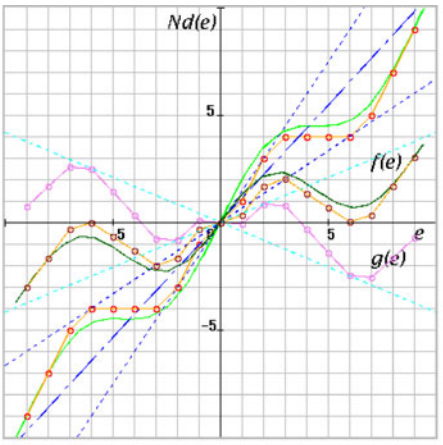

(a)

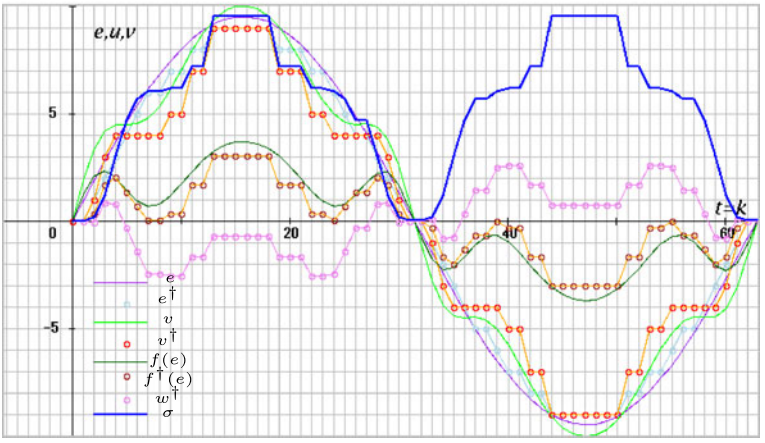

(b)

Fig. 2.25 Discretized input/output signals of a nonlinear element for Example 2.2

Example 2.2 For the example of Figs. 2.25(a) and (b), the following nonlinear characteristic is considered:

$$\begin{aligned} e^{\dagger} &= \gamma * (\texttt{double})(\texttt{int})(e/\gamma) \\ v &= 1.0 * e^{\dagger} + 1.5 * \texttt{sin}(0.7 * e^{\dagger}) \\ v^{\dagger} &= \gamma * (\texttt{double})(\texttt{int})(v/\gamma). \end{aligned} \tag{2.45}$$

The second equation of (2.45) is an inclined sinusoidal function. In either of the examples, (2.41) in Lemma 2.4 is satisfied, i.e., $\sigma(k) \geq 0$ $(k = 1, 2, \cdots)$.

Figures 2.26(a), (b) and 2.27(a), (b) show the two cases in Examples 2.1 and 2.2 with a nearly continuous characteristic, where $\gamma = 0.1$ and $h = 0.1$, that is, $1/10$ *high resolution*. As is obvious from the figures, $\sigma(t) \geq 0$ $(t = 0.1, 0.2, \cdots)$. Thus,

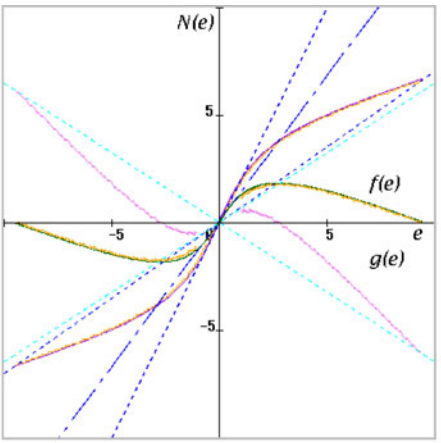

(a)

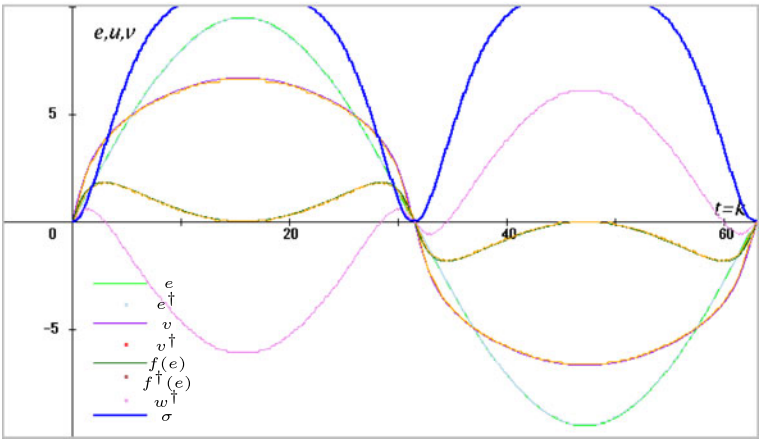

(b)

Fig. 2.26 Input/output signals of a nearly continuous characteristic for Example 2.1

the calculated results show that the input/output characteristics of nonlinear elements become similar to continuous problems, that is, Popov's criterion and other conditions in continuous time.

Example 2.3 Figures 2.28(a) and (b) illustrate the case where the following nearly nonlinear characteristic is considered:

$$\begin{aligned} e^{\dagger} &= \gamma * (\texttt{double})(\texttt{int})(e/\gamma) \\ v &= 1.0 * e^{\dagger} + 0.15 * \texttt{sin}(0.7 * e^{\dagger}) \\ v^{\dagger} &= \gamma * (\texttt{double})(\texttt{int})(v/\gamma). \end{aligned} \tag{2.46}$$

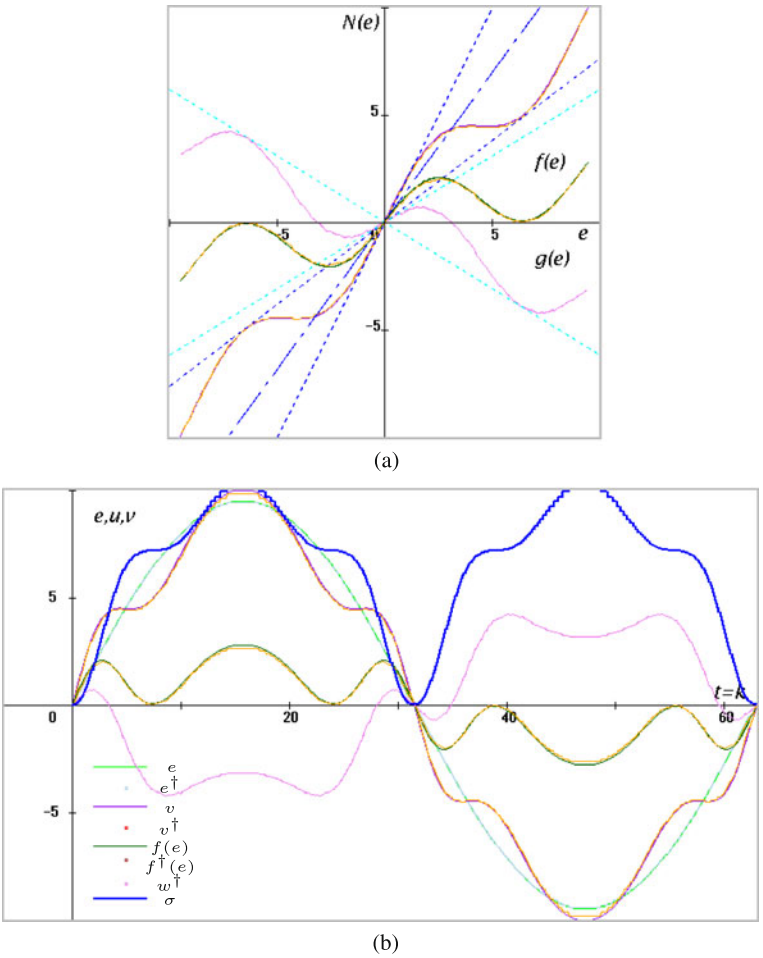

Fig. 2.27 Input/output signals of a nearly continuous characteristic for Example 2.2

In this example, the amplitude of sinusoidal function is chosen as $1/10$ for Example 2.2 (i.e., $1.5 \rightarrow 0.15$). Figures 2.29(a) and (b) illustrate the case where $1/10$ high resolution is applied (i.e., $\gamma = 0.1$ and $h = 0.1$). As is obvious from these examples, the theory of discretized static and/or dynamic nonlinear systems (in other words, discrete-time and discrete-value nonlinear systems) considered in this chapter approaches that of continuous-time and continuous-value nonlinear systems asymptotically for $\gamma \rightarrow 0$ and $h \rightarrow 0$. Of course, it includes that of continuous linear systems for $\beta \rightarrow 0$ naturally, as shown in Figs. 2.29(a) and (b).

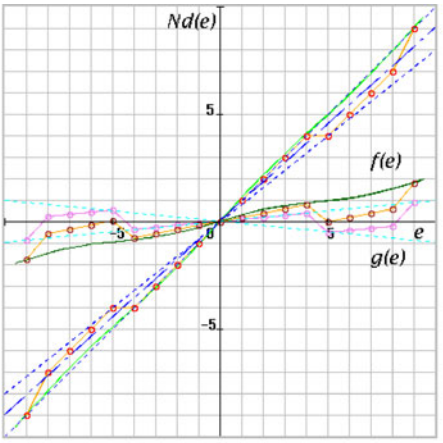

(a)

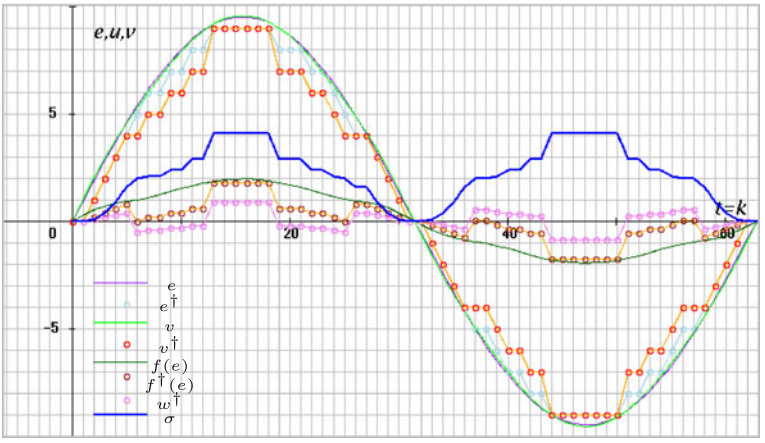

(b)

Fig. 2.28 Discretized input/output signals of a nearly continuous characteristic for Example 2.3

2.7 Exercises

(1) Prove that the sector condition in (2.5),

$$|g(e)| \leq \beta |e|,$$

is equivalently written as (2.7).

(2) Confirm that block diagram Fig. 2.16 is equivalent to Fig. 2.15.

(3) From Fig. 2.18, determine the loop transfer function $H(\beta, q, z)$ in Fig. 2.19.

(4) From (2.5) and (2.29), prove the sector inequality in (2.31), that is,

$$0 \leq \frac{f(e(k))}{e(k)} \leq 2\beta.$$

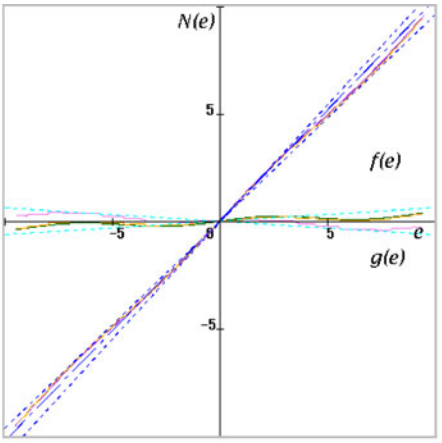

(a)

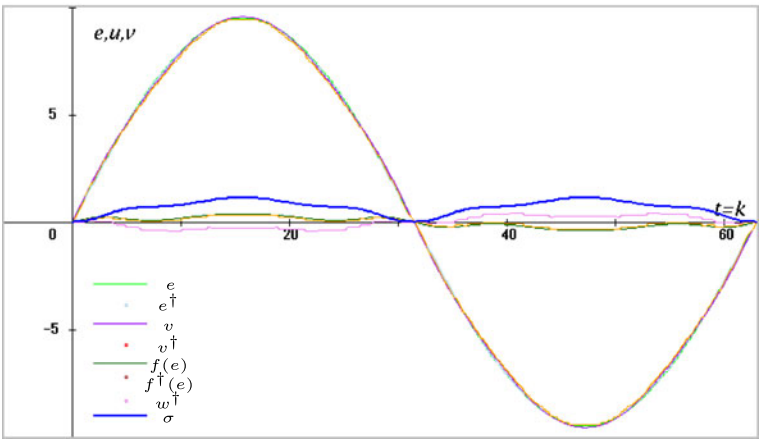

(b)

Fig. 2.29 Discretized input/output signals of a nearly continuous characteristic for Example 2.3

(5) Prove Lemma 2.1, that is,

$$\|\overline{w}^{\dagger}(k)\|_{2,N} \leq \beta \|\overline{e}^{\dagger}(k)\|_{2,N} \leq \beta \|\overline{e}(k)\|_{2,N},$$

using inequality (2.34).

(6) For $N = 2$, prove Schwarz's inequality (2.60).

(7) Using the result of (6), prove Minkowski's inequality (2.68) when $N = 2$.

Appendix A: Norms and Inner Products of L_p and ℓ_p Spaces

In this appendix, inner products and norms in an ℓ_2 space are explained for discrete-time systems. In general, norms of L_p and ℓ_p spaces are defined as follows. For a continuous-time signal $x\colon \mathbb{R}_+ \to \mathbb{R}$,

$$\|x(t)\|_p := \left(\int_0^\infty |x(t)|^p dt\right)^{1/p}, \quad 1 \le p < \infty, \tag{2.47}$$

$$\|x(t)\|_\infty := \operatorname*{ess\,sup}_{t\in[0,\infty)} |x(t)|, \tag{2.48}$$

and for a discrete-time signal $x\colon \mathbb{Z}_+ \to \mathbb{R}$ (or $\mathbb{Z}$),

$$\|x(k)\|_p := \left(\sum_{k=1}^\infty |x(k)|^p\right)^{1/p}, \quad 1 \le p < \infty, \tag{2.49}$$

$$\|x(k)\|_\infty := \sup_{k\ge 1} |x(k)|. \tag{2.50}$$

In the ℓ_2 space, the norm is defined as

$$\|x(k)\|_2 := \left(\sum_{k=1}^\infty |x(k)|^2\right)^{1/2}, \tag{2.51}$$

and the inner product is given by

$$\langle x(k), y(k)\rangle := \sum_{k=1}^\infty x(k)y(k). \tag{2.52}$$

The preceding definitions for finite time series $x(k)(k = 0, 1, 2, \cdots, N)$ are written as follows:

$$\|x(k)\|_{2,N} := \left(\sum_{k=1}^N |x(k)|^2\right)^{1/2}, \tag{2.53}$$

$$\langle x(k), y(k)\rangle_N := \sum_{k=1}^N x(k)y(k). \tag{2.54}$$

When $N \to \infty$, these definitions are written as:

$$\|x(k)\|_2 := \lim_{N\to\infty} \|x(k)\|_{2,N}, \tag{2.55}$$

$$\langle x(k), y(k)\rangle := \lim_{N\to\infty} \langle x(k), y(k)\rangle_N. \tag{2.56}$$

Appendix B: Hölder and Schwarz Inequalities

(1) In an L_p space, the following inequality holds:

$$\int_0^\infty |x(t)y(t)|\mathrm{d}t \le \left(\int_0^\infty |x(t)|^p \mathrm{d}t\right)^{1/p} \left(\int_0^\infty |y(t)|^q \mathrm{d}t\right)^{1/q}, \quad \frac{1}{p}+\frac{1}{q}=1. \tag{2.57}$$

As for discrete signals, the following inequality holds in an ℓ_p space:

$$\sum_{k=1}^\infty |x(k)y(k)| \le \left(\sum_{k=1}^\infty |x(k)|^p\right)^{1/p} \left(\sum_{k=1}^\infty |y(k)|^q\right)^{1/q}, \quad \frac{1}{p}+\frac{1}{q}=1. \tag{2.58}$$

These are called Hölder's inequalities [4, 8, 10]. The proof is given for $1 \le p \le \infty$ (i.e., $1 \le q \le \infty$) in, e.g., [8].

(2) An important special case of (2.58) for $p = q = 2$ is given as

$$\sum_{k=1}^\infty |x(k)y(k)| \le \left(\sum_{k=1}^\infty |x(k)|^2\right)^{1/2} \left(\sum_{k=1}^\infty |y(k)|^2\right)^{1/2}. \tag{2.59}$$

Equation (2.59) is called Schwarz's inequality. The easier proof of (2.59) is as follows. For finite sums of N steps, Schwarz's inequality (2.59) is rewritten as

$$\left(\sum_{k=1}^N |x(k)y(k)|\right)^2 \le \left(\sum_{k=1}^N |x(k)|^2\right)\left(\sum_{k=1}^N |y(k)|^2\right) \tag{2.60}$$

$$\sum_{k=1}^N |x(k)y(k)|^2 + 2\sum_{k,l=1,k\ne l}^N |x(k)y(k)|\cdot|x(l)y(l)|$$

$$\le \sum_{k=1}^N |x(k)|^2|y(k)|^2 + \sum_{k,l=1,k\ne l}^N |x(k)|^2|y(l)|^2. \tag{2.61}$$

In (2.61), the following sum must be non-negative:

$$\sum_{k,l=1,k\ne l}^N |x(k)|^2|y(l)|^2 - 2\sum_{k,l=1,k\ne l}^N |x(k)y(k)|\cdot|x(l)y(l)| = \left(\sum_{k,l=1,k\ne l}^N |x(k)y(l)|\right)^2, \tag{2.62}$$

and it must hold for $N \to \infty$. Thus, inequality (2.60) has been proved.

Appendix C: Minkowski Inequalities

(1) In an L_p space, the following inequality holds:

$$\left(\int_0^\infty |x(t)+y(t)|^p \mathrm{d}t\right)^{1/p} \le \left(\int_0^\infty |x(t)|^p \mathrm{d}t\right)^{1/p} + \left(\int_0^\infty |y(t)|^p \mathrm{d}t\right)^{1/p}. \tag{2.63}$$

The norm expression based on (2.47) is given by

$$\|x(t)+y(t)\|_p \le \|x(t)\|_p + \|y(t)\|_p. \tag{2.64}$$

As for discrete signals, the following inequality holds in an ℓ_p space:

$$\left(\sum_{k=1}^\infty |x(k)+y(k)|^p\right)^{1/p} \le \left(\sum_{k=1}^\infty |x(k)|^p\right)^{1/p} + \left(\sum_{k=1}^\infty |y(k)|^p\right)^{1/p}. \tag{2.65}$$

The norm expression based on (2.49) is given by

$$\|x(k)+y(k)\|_p \le \|x(k)\|_p + \|y(k)\|_p. \tag{2.66}$$

These are called Minkowski's inequalities [7, 8].

(2) A special case of (2.65) for $p=2$ and finite sums of N steps is written as

$$\left(\sum_{k=1}^N |x(k)+y(k)|^2\right)^{1/2} \le \left(\sum_{k=1}^N |x(k)|^2\right)^{1/2} + \left(\sum_{k=1}^N |y(k)|^2\right)^{1/2} \tag{2.67}$$

$$\|x(k)+y(k)\|_{2,N} \le \|x(k)\|_{2,N} + \|y(k)\|_{2,N}. \tag{2.68}$$

In order to prove (2.65), consider the following equality:

$$(|x(k)|+|y(k)|)^p = |x(k)|(|x(k)|+|y(k)|)^{p-1} + |y(k)|(|x(k)|+|y(k)|)^{p-1}.$$

Hölder's inequality gives

$$\sum_{k=1}^N |x(k)|(|x(k)|+|y(k)|)^{p-1} \le \left(\sum_{k=1}^N |x(k)|^p\right)^{1/p} \left(\sum_{k=1}^N (|x(k)|+|y(k)|)^{(p-1)q}\right)^{1/q} \tag{2.69}$$

$$\sum_{k=1}^N |y(k)|(|x(k)|+|y(k)|)^{p-1} \le \left(\sum_{k=1}^N |y(k)|^p\right)^{1/p} \left(\sum_{k=1}^N (|x(k)|+|y(k)|)^{(p-1)q}\right)^{1/q}. \tag{2.70}$$

Since $(p-1)q = p$ and $1/q = 1 - 1/p$, the addition of (2.70) and (2.69) gives

$$\sum_{k=1}^{N}(|x(k)| + |y(k)|)^p \le \left(\sum_{k=1}^{N}(|x(k)| + |y(k)|)^p\right)^{(1-1/p)} \cdot \left[\left(\sum_{k=1}^{N}|x(k)|^p\right)^{1/p} + \left(\sum_{k=1}^{N}|y(k)|^p\right)^{1/p}\right]. \tag{2.71}$$

Moreover, $|x(k) + y(k)| \le |x(k)| + |y(k)|$. Thus, Minkowski's inequality (2.65) is obtained for $N \to \infty$.

To provide a clear understanding, the following simple equality is considered here:

$$(|x(k)| + |y(k)|)^2 = |x(k)|(|x(k)| + |y(k)|) + |y(k)|(|x(k)| + |y(k)|).$$

Schwarz's inequality gives

$$\begin{aligned}&|x(1)|(|x(1)| + |y(1)|) + |x(2)|(|x(2)| + |y(2)|)\\ &\le (|x(1)|^2 + |x(2)|^2)^{1/2}[(|x(1)| + |y(1)|)^2 + (|x(2)| + |y(2)|)^2]^{1/2}\end{aligned}$$

$$\begin{aligned}&|y(1)|(|x(1)| + |y(1)|) + |y(2)|(|x(2)| + |y(2)|)\\ &\le (|y(1)|^2 + |y(2)|^2)^{1/2}[(|x(1)| + |y(1)|)^2 + (|x(2)| + |y(2)|)^2]^{1/2}.\end{aligned}$$

By adding these inequalities, we have

$$\begin{aligned}&(|x(1)| + |y(1)|)^2 + (|x(2)| + |y(2)|)^2\\ &\le [(|x(1)|^2 + |x(2)|^2)^{1/2} + (|y(1)|^2 + |y(2)|^2)^{1/2}]\\ &\qquad \cdot [(|x(1)| + |y(1)|)^2 + (|x(2)| + |y(2)|)^2]^{1/2}.\end{aligned}$$

Thus,

$$\sqrt{|x(1) + y(1)|^2 + |x(2) + y(2)|^2} \le \sqrt{|x(1)|^2 + |x(2)|^2} + \sqrt{|y(1)|^2 + |y(2)|^2},$$

and the equality problem is proved.

References

1. Bartoszewicz A (ed) (2011) Robust control, theory and applications. InTech, Rijeka, pp 243–260, Chap 11
2. Harris CJ, Valenca JME (1983) The stability of input-output dynamical systems. Academic Press, New York
3. Kalman RE (1956) Nonlinear aspects of sampled-data control systems. In: Proc of the symposium on nonlinear circuit analysis, vol VI, pp 273–313

4. Mashreghi J (2009) Representation theorem in Hardy spaces. Cambridge University Press, Cambridge
5. Okuyama Y (2006) Robust stability analysis for discretized nonlinear control systems in a global sense. In: Proc of the 2006 American control conference, Minneapolis, MN, USA, pp 2321–2326
6. Okuyama Y (2008) Discretized PID control and robust stabilization for continuous plants. In: Proc of the 17th IFAC world congress, Seoul, Korea, pp 1492–1498
7. Royden HL (1988) Real analysis, 3rd edn. Prentice-Hall, New York
8. Rudin W (1987) Real and complex analysis, 3rd edn. McGraw-Hill, New York
9. Vidyasagar M (1993) Nonlinear systems analysis, 2nd edn. Prentice-Hall, New York, republished by SIAM, 2002
10. Yosida K (1980) Functional analysis, 6th edn. Springer, Berlin

http://www.springer.com/978-1-4471-5666-6

Discrete Control Systems
Okuyama, Y.
2014, XII, 251 p. 165 illus., 100 illus. in color.,
Hardcover
ISBN: 978-1-4471-5666-6